This electronic companion is part of the manuscript entitled **"An integrated tool for optimal energy scheduling and power quality improvement of a smart grid under multiple demand response schemes"** which has been exclusively submitted to **Applied Energy** for publication.

Appendix A. Short line model

Let us consider a short single-phase line from the bus 1 to bus 2. In a microgrid, bus 1 could represent a DG and the bus 2 the AC bus of the microgrid. The real part of the voltage difference ΔV_d and the imaginary part ΔV_q are approximated by the equations A.1 and A.2.

$$\Delta V_d = \frac{RP_1 + XQ_1}{V_1} \simeq V_1 - V_2 \tag{A.1}$$

$$\Delta V_q = \frac{XP_1 - RQ_1}{V_1} \simeq V_2\delta \tag{A.2}$$

Equation A.1 represents the voltage drop from bus 1 to bus 2. It is clearly shown that voltage drop is highly dependent on the reactive power flow for inductive lines. Equation A.2 shows on the contrary that the angle in radian δ between the two buses will be highly dependent on the active power flow for inductive lines. However, both the active and reactive powers have an impact on the voltage drop and the angle δ. Figures A.12 and A.13 show the notations and the vectorial representation of the voltages, impedance and current in the circuit.

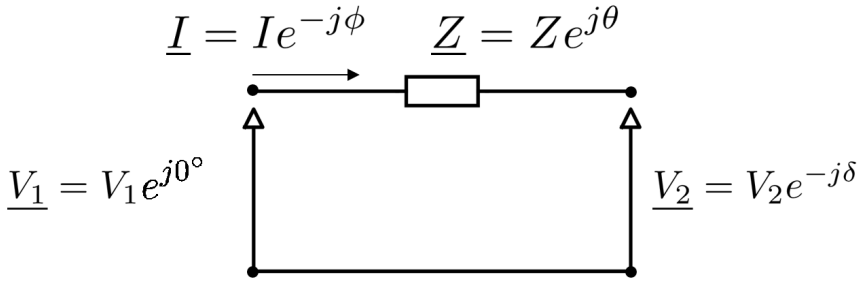

Figure A.12: Short line model (single phase)

In bus 1,

$$\begin{aligned} P_1 &= \Re\left\{\underline{V_1}\underline{I}^*\right\} \quad \text{with} \quad \underline{I}^* = \frac{\underline{V_1}^* - \underline{V_2}^*}{\underline{Z}^*} \\ &= \frac{V_1^2}{Z}\cos(\theta) - \frac{V_1 V_2}{Z}\cos(\delta+\theta) \\ &= \frac{V_1}{Z}\cos(\theta)\underbrace{(V_1 - V_2\cos(\delta))}_{\Delta V_d} + \frac{V_1}{Z}\underbrace{V_2\sin(\delta)}_{\Delta V_q}\sin(\theta) \end{aligned} \tag{A.3}$$

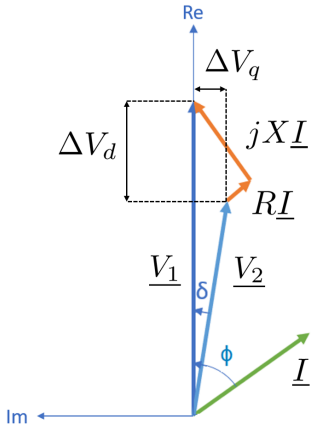

Figure A.13: Complex phasors representation.

Similarly, we find

$$\begin{aligned} Q_1 &= \Im\left\{\underline{V_1}\underline{I}^*\right\} \\ &= \frac{V_1}{Z}\sin(\theta)\underbrace{(V_1 - V_2\cos(\delta))}_{\Delta V_d} - \frac{V_1}{Z}\underbrace{V_2\sin(\delta)}_{\Delta V_q}\sin(\theta) \end{aligned} \tag{A.4}$$

By rearranging A.3 and A.4 and developing $\underline{Z}$ in $R + jX$, we find

$$\Delta V_d = \frac{RP_1 + XQ_1}{V_1} \tag{A.5}$$

$$\Delta V_q = \frac{XP_1 - RQ_1}{V_1} \tag{A.6}$$

Equations A.1 and A.2 form a system of two equations with two unknown variable where ΔV_d and ΔV_q represent the direct and quadrature value of the voltage deviation in the complex frame. If we consider short lines, phase angle δ between the buses 1 and 2 is relatively low and we can find that

$$\Delta V_d = \frac{RP_1 + XQ_1}{V_1} \triangleq V_1 - V_2\underbrace{\cos(\delta)}_{\simeq 1} \simeq V_1 - V_2 \tag{A.7}$$

$$\Delta V_q = \frac{XP_1 - RQ_1}{V_1} \triangleq V_2\underbrace{\sin(\delta)}_{\simeq \delta} \simeq V_2\delta \tag{A.8}$$

Appendix B. Microgrid test case

The utility grid seen from the PCC can be replaced by its Thevenin equivalent impedance and voltage source. The utility grid considered has a short-circuit impedance of 1000 MVA and X/R ratio of 22. The loss parameters $loss_P$ and $loss_Q$, based on which P_t^{loss} and Q_t^{loss}

are calculated in Eq. (6), are tuned to the upper bound of the ratio between the total active (or reactive) loss with respect to the active (or reactive) total load. After several trials, $loss_P$ is set at 1.5% and $loss_Q$ is set at 13.0%.

Transformers and lines

The properties concerning the transformers and the lines of the MG are specified in Tables B.2 and B.3.

Table B.2: Properties of the transformers

Transformers	Voltage	Base KVA	Connection	%Z	X/R
T_1	0.4/11.2 kV	750	Δ-Y	5.75	6
T_2, T_3, T_4	11.2/0.4 kV	200	Δ-Y	5.75	6

Table B.3: Properties of the lines

Lines	Voltage	Length	Type	r	x
$L121-2$	0.4 kV	0.05 km	3 phases/4 wires	$0.049\,\Omega\,\mathrm{km}^{-1}$	$0.027\,\Omega\,\mathrm{km}^{-1}$
$L131-3$	0.4 kV	0.15 km	3 phase/4 wires	$0.049\,\Omega\,\mathrm{km}^{-1}$	$0.027\,\Omega\,\mathrm{km}^{-1}$
$L3-6$	0.23 kV	0.4 km	3 phase/4 wires	$0.06\,\Omega\,\mathrm{km}^{-1}$	$0.03\,\Omega\,\mathrm{km}^{-1}$
$L171-7$	0.4 kV	0.15 km	3 phases/4 wires	$0.049\,\Omega\,\mathrm{km}^{-1}$	$0.027\,\Omega\,\mathrm{km}^{-1}$
$L181-8$	0.4 kV	0.40 km	3 phases/4 wires	$0.06\,\Omega\,\mathrm{km}^{-1}$	$0.03\,\Omega\,\mathrm{km}^{-1}$
$L8-10$	0.4 kV	0.2 km	3 phase/4 wires	$0.049\,\Omega\,\mathrm{km}^{-1}$	$0.027\,\Omega\,\mathrm{km}^{-1}$

Appendix C. Distributed energy resources

Technical properties

The technical properties concerning the DERs and the ES are shown in Tables C.4 and C.5.

Table C.4: Technical properties of the distributed generators

DER	Apparent power	$P_{r,t}^{\mathrm{DG,min}}$	$P_{r,t}^{\mathrm{DG,max}}$	$Q_{r,t}^{\mathrm{DG,max}}$	Max PF
APS1,APS2	250 kVA	50 kW	200 kW	150 kVAR	0.8
WP	95 kVA	0 kW	85 kW	40 kVAR	0.9
PV	165 kVA	0 kW	147 kW	71 kVAR	0.9

We also assume that all DERs are interfaced with a two or four-quadrant converter. Since the electronic switches of these converters are generally commanded with a PWM scheme, the low current harmonics that the converter generates have a small magnitude and be neglected. For the high frequency harmonics, they can be filtered rather effectively with an appropriate filter. For those reasons, it is assumed that the DERs operate ideally, at the base frequency of 50 Hz.

The EVs specifications are provided in Table C.6 below:

Table C.5: Properties of energy storage

Storage	Capacity	$P_s^{\max,ch/dis}$	$Q_s^{\max}$	Efficiency	Res. ener. value $\tilde{\varepsilon}$	Max PF
ES	80 kWh	40 kW	37 kVAR	90%	0.147 \$/kWh	0.85

Table C.6: Properties of EVs

Model	Capacity	$P^{\text{EV,max,ch/dis}}$	Minimum SoE	Efficiency
Nissan Leaf	24 kWh	7.68 kW	4.8 kWh	90%

Economic properties

The cost-related data for the DERs are presented in this section. Table C.7 shows the operational and start-up costs for each DER.

Table C.7: Economic properties of the distributed generators

DER	Operational cost $C_r^{\text{DG,op}}$	Start-up cost C_r^{ST}
APS1,APS2	0.26 \$/kWh	8 \$/kWh
WP	0.01 \$/kWh	0 \$/kWh
PV	0.01 \$/kWh	0 \$/kWh

As already mentioned, we have also introduced a battery degradation cost to avoid unnecessary charging/discharging of the ES and the EVs and at the same time, incentivize the system to prioritize energy from renewables first. For both ES and EVs, the penalty cost equals to 0.001 \$/kWh. We have also considered a small penalty to mitigate reactive power exchange among the DERs of the microgrid and between the microgrid and the main grid. The value for these penalties is $C^{\text{grid,react.}} = C^{\text{DER,react.}} = 0.0001\$/\text{kVAR}$.

Renewable generation

As it has been already mentioned, the wind and solar generation data should reflect their forecasts. For the PV curve, we have used an average of one year measurements data from smart meters installed in Walloon region, Belgium. The wind data were generated by a stochastic algorithm based on a Weibull probabilistic distribution. The original wind speed measurements used to create the Weibull distribution were recorded at Saint-Hubert in Belgium by the Belgian Royal Institute of Meteorology. Fig. C.14 below illustrates the PV and wind energy generation used in this study.

Appendix D. Loads

Loads composition

As mentioned in Section 3.1, to represent the diversity of loads present in the system, each aggregated Load at a node of the microgrid consists of several load types, depending on

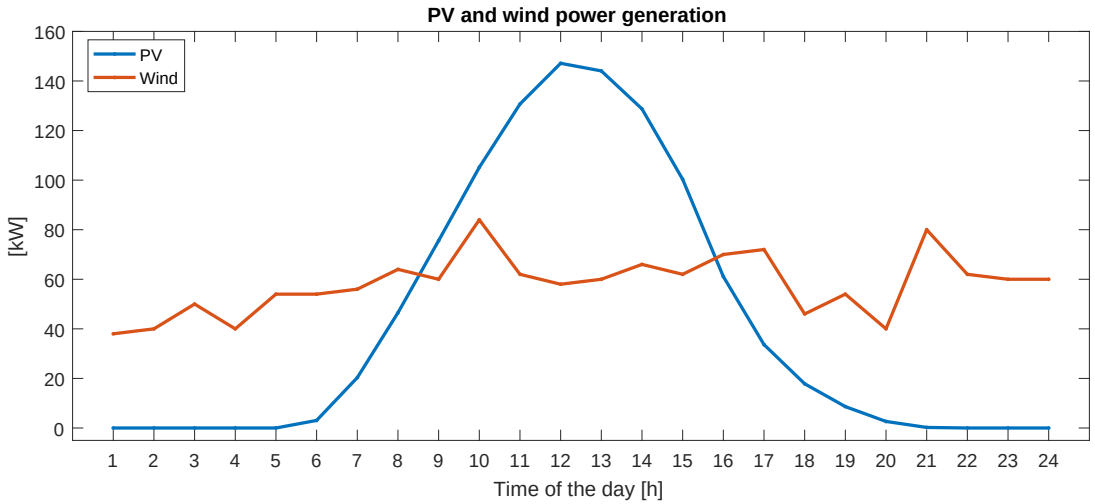

Figure C.14: Forecasts for PV and wind power generation

their end-use. Figure D.15 illustrates the average composition of residential, commercial and industrial loads in the United States according to the U.S. Energy Information Administration (EIA) [38]. The agency mentions that "all other uses" in the residential and industrial loads include the *many, mostly small, appliances in U.S. homes, apartments, and related property* [38]. All the aggregated loads are assumed to be balanced in a first approach.

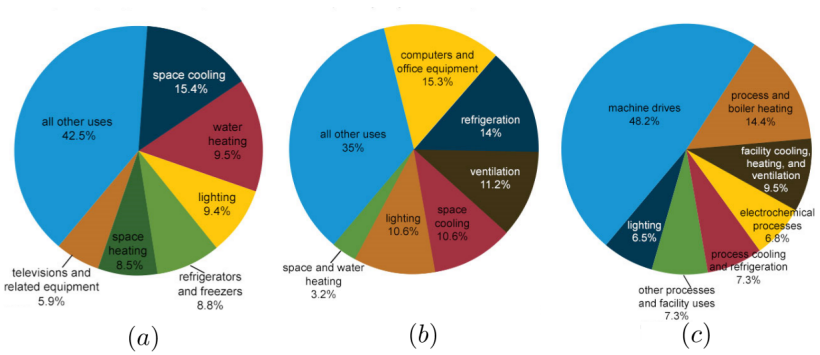

(a) (b) (c)

Figure D.15: Average composition of residential (a), commercial (b) and industrial (c) loads [38]

Based on the aforementioned statistics, Table D.8 presents the composition of the individual load types considered in the three aggregated loads of the microgrid. The first load at node 6 (Load 1) is residential and it mainly consists of appliances and HVAC. A big share of the industrial Load 2 at node 7, is due to the machine drives consuming their necessary power to operate during the day. Load 3 represents a complex of small office buildings operating mainly during business hours.

Table D.8: Parameter $\eta_{l,ty}^{\text{type,load}}$ for the different loads and end-uses [38].

Load	HVAC	DHW	Lights	Appliances	Motor drives
Load 1	23.9%	9.5%	9.4%	57.2%	0%
Load 2	16.8%	14.4%	6.5%	7.3%	55%
Load 3	37.3%	1.8%	10.6%	50.3%	0%

Harmonic survey

This study assumes that every type of load has a constant spectrum. Figure D.16 shows an example of the magnitude of the odd current harmonics for the devices of the "appliance" type. The average magnitude for each current harmonic is found by adding the spectrum of each equipment, weighted by its consumption share inside the load type. Figure D.17 displays the average consumption shares for the appliances. Finally, Table D.9 synthesizes this information for every type of load.

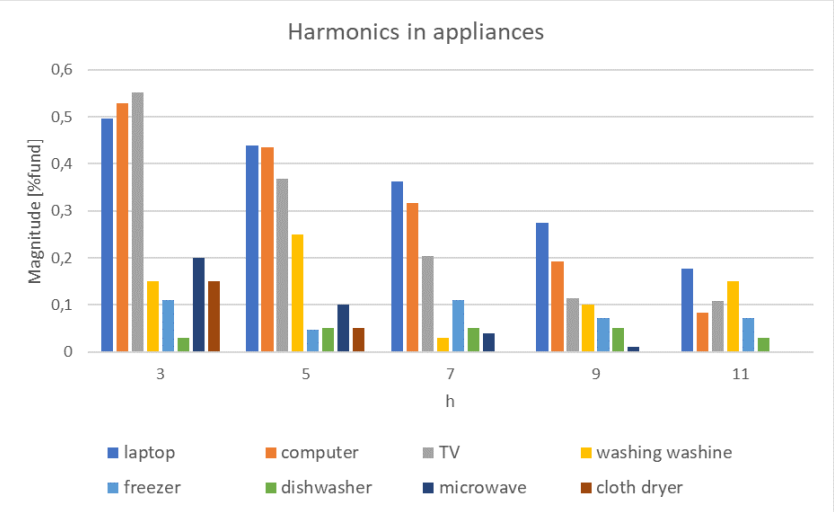

Figure D.16: Magnitude of odd current harmonics with respect to the fundamental for different appliances [33]

Aggregated loads

In this Section, we provide the load curves and detailed information regarding the three aggregated loads considered in this microgrid model. Load 1 (located at Node 6) is a residential load composed of different households and with a consumption profile of Western European families. The total hourly consumption trend during a day was simulated with the CREST Demand Model. This open-source model uses a stochastic bottom-up approach and was developed by the Centre for Renewable Energy Systems Technology of the Loughborough University [39]. Load 2 located at node 7 represents an industrial profile composed of some

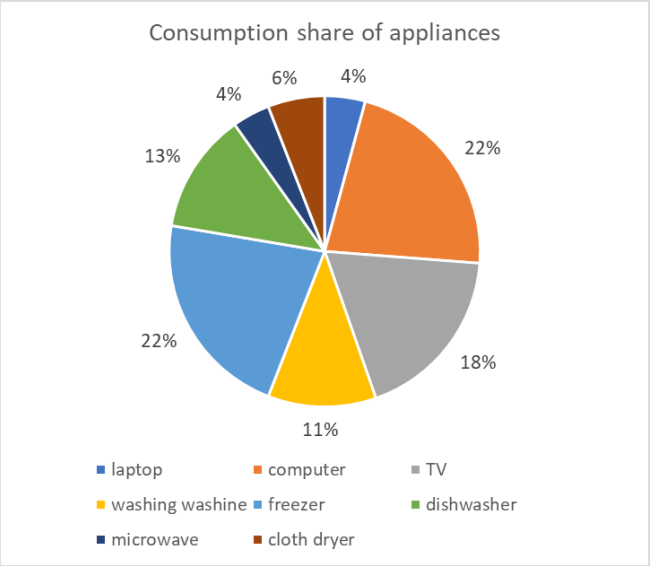

Figure D.17: Average demand share of each device inside the appliance load type [33, 32]

Table D.9: Single current harmonic magnitude with respect to the fundamental, current THD and power factor per type of load [32, 34, 33].

	Current harmonic magnitude				
h	HVAC	DHW	Lights	Appliances	Motor drives
3	5.0%	0%	21.1%	29.9%	0%
5	6.0%	0%	11.9%	23.3%	0%
7	2.3%	0%	11.8%	15.7%	0%
9	1%	0%	2%	10.8%	0%
11	0%	0%	1%	8.2%	0%
THD_I	8.2%	0%	27.1%	43.3%	0%
pf	0.98	1	0.8	0.65	1

offices and a workshop. The original data used for the modelling of this load come from real measurements of energy meters on a firm with some offices and an industrial painting workshop in Belgium. Finally, Load 3 located at node 8 represents a small complex of company office buildings. Fig. D.18 illustrates the load curves for all three aggregated loads.

Economic properties

As mentioned in Section 2, we have introduced the concept of the value of lost load (VOLL) to prioritize the loads that the energy management system can defer or shed, and which result in the least additional cost for the system. A higher VOLL value indicates a more valuable (sensitive) load and thus, it is more expensive for the system to constrain

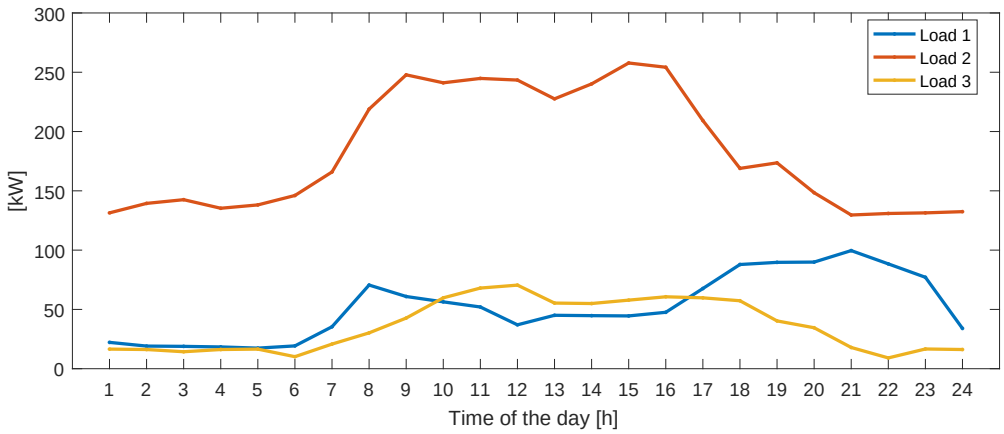

Figure D.18: The three aggregated loads used in microgrid test case

it. Table D.10 presents the considered VOLL values for each load type, as well as the their maximum reduction capability the EMS can use.

Table D.10: VoLL and reduction capability for the different types of load

Type of load	VoLL	Reduction capability
HVAC	0.3$/kWh	20%
DHW	0.35$/kWh	20%
Lights	0.55$/kWh	10%
Appliances	0.55$/kWh	15%
Motor drives	0.85$/kWh	1%